DOI: 10.1002/fuce.200900114

Effects of GDL Structure with an Efficient Approach to the Management of Liquid water in PEM Fuel Cells

Erin E. Kimball[1]*, Jay B. Benziger[1], Yannis G. Kevrekidis[1]

[1] Department of Chemical Engineering Princeton University, Princeton, NJ 08544, United States

Received June 5, 2009; accepted December 11, 2009

Abstract

A model fuel cell with a single transparent straight flow channel and segmented anode was constructed to measure the direct correlation of liquid water movement with the local currents along the flow channel. Water drops emerge through the largest pores of the GDL with the size of the droplets that emerge on the surface determined by the size of the pore and its location under the gas flow channel or under the land. Gravity, surface tension, and the shearing force from the gas flow control the movement of liquid in the gas flow channel. By creating a single large diameter pore in the GDL, liquid water flow emergent from the GDL was forced to be in specific locations along the length of the channel and either under the land or under the channel. The effects of gravity were amplified when the large pore was under the channel, but diminished with the large pore under the land. Current fluctuations were minimised when the dominant water transport from the GDL pore was near the cathode outlet. The results show that it is possible to engineer the water distribution in PEM fuel cells by modifying the pore sizes in the GDL.

Keywords: GDL, MEA, Model Fuel Cell, PEM Fuel Cells, Water Management

1 Introduction

The economic, environmental, and political implications of a dwindling supply of fossil fuels are immense and cannot be ignored. Sustaining the world's growing energy demands will require the development and widespread implementation of alternative energy sources. Polymer electrolyte membrane (PEM) fuel cells are part of the broad picture as energy conversion devices that utilise hydrogen as fuel and produce only water. Their low temperature operation and flexibility in design make them well suited for portable, stationary, and automotive applications, provided that the fuel cell itself and the balance of plant can be made sufficiently robust and reliable. One of the most important engineering hurdles for PEM fuel cells to meet these requirements is the efficient management of water. There must be enough water to hydrate the membrane due to the exponential dependence of the proton conductivity on water activity [1]. Humidifiers are commonly used to add water vapour to the feed gases to keep the membrane hydrated. The humidifiers add complexity to the fuel cell system as they must be properly controlled for temperature and gas flow rate. Formation of water as a reaction product in the fuel cell causes super-saturation conditions to exist and liquid water condenses, causing 'flooding', or the accumulation of liquid water in the flow channels. Flooding hinders the transport of reactants from the flow channels into the gas diffusion layer (GDL) and to the catalyst/membrane interface where the electrochemical reaction takes place. A common solution to reduce flooding is to increase the flow rates of the reactant gases so that excess water is simply blown out of the fuel cell [2–4]. However, the large excess gas flow requires highly humidified gas feeds to prevent the evaporation of too much water from the membrane, beginning near the inlets and creating a drying front that causes the membrane conductivity to become insufficient.[5–8] The high gas flows also reduce fuel conversion and frequently require recycling to improve utilisation. Both of these are a significant addition to the cost, complexity, and parasitic power losses of the system.

[*] *Corresponding author, ekimball@princeton.edu*

Several groups have investigated the transport of liquid water through the GDL and flow channels using techniques varying from direct visualisation[9] to neutron[4] and magnetic resonance [10] imaging to *ex situ* experiments with fluorescence microscopy [11]. Although, the collection of observations provides a better understanding of some of the most important physics for flooding and water transport, there has been little progress in utilising this knowledge to improve the design and operation of PEM fuel cells. To our knowledge, only one other group has tried to use the substantial body of research on liquid water build-up in a novel design of the GDL [12]. In their work, they used a laser to carve large pores, about 80 μm in diameter, out of a carbon paper GDL at multiple points under the flow channel. By comparing polarisation curves and overpotentials, they determined that the perforated GDL did improve the fuel cell performance even though the internal impedance of the fuel cell increased. They postulated that the large pores sucked water from the surrounding smaller pores because of differences in capillary pressure, but they did not comment on any changes in hydrophobicity of the large pores caused by the laser beam.

In the present work we explore the basic physics of coupling liquid flow in the gas diffusion layer and liquid flow in the gas flow channel. In order to develop better, more efficient designs, it is necessary to first understand the physics that control water generation and motion in PEM fuel cells and identify the system parameters that can be engineered into the system. With this goal, earlier work in our group first showed that the water produced by the electrochemical reaction is more than sufficient for hydrating the membrane; it is the small flow channels and high gas velocities that reduce the back mixing of water in the fuel cell that allows for autohumidified operation with dry feeds [13]. Next, we provided evidence for the importance of gravity for liquid water motion and the influence on local current density; liquid water droplets emerging from the GDL either detach and fall when gravity overcomes the surface tension holding the drop to the pore or accumulate and block the pore openings, depending on the orientation of the flow channels [14]. The size of water drops and slugs in the gas flow channels result from a balance of local current density, pore sizes in the GDL, the gravitational force, the shear force from the gas flows, and the dimensions of the flow channel. A change in one of these parameters alters the conditions when a water drop spans the flow channel and blocks the reactant flow, thus changing the dynamics of the fuel cell operation.

Here we report on the next step: can we take advantage of mixing and gravitational forces so that the correct flow and distribution of water in the fuel cell be engineered without the burden of extra equipment? In this work we have focused on the structure of the GDL as a possible factor in the answer. Two different GDL materials, carbon cloth and carbon paper, with different intrinsic pore size distributions, were compared through the effects of gravity and gas flow rate on the local current measurements. The pore sizes controlled the size of the droplets that formed before detaching from the surface of the GDL. We observed very different behaviour depending on whether droplets detached from the pore or formed a slug first. We then investigated the effects of choosing where the droplets emerged at the GDL surface. This was done by taking advantage of the hydrophobicity of the GDL (the property that causes liquid water to flow through only the largest pores; see [14]) and forcing a single pore larger than the intrinsic pore sizes to be in a certain location. The pore could be under the channel or under the land, and closer to the inlets or closer to the outlets. The results presented here show that the optimal choice is actually specific to the application of the fuel cell system, and is significantly altered by the flow channel orientation and effects of gravity.

2 Experimental Methods

2.1 SAPC Fuel Cell

The experiments were conducted with the segmented anode, parallel channel (SAPC) fuel cell, described elsewhere [8]. Briefly, the particular fuel cell used in the experiments presented here consisted of two transparent polycarbonate plates with flow channels 1.6 mm wide × 3.2 mm deep × 75 mm long. The flow channels are about a factor of 2 larger than what is commonly described in the literature as this allows us to better isolate the influence of gravity and local variations apart from the shear force and pressure from the gas flows. The design was such that the anode and cathode flow channels were in a single plane and terminated in a 90° angle that connected into a tube fitting adapted to 1/8″ polyethylene tubing. A CCD camera was positioned to view the cathode flow channel. (We also viewed the anode flow channel, but all the interesting phenomena were observed at the cathode). Video images were collected and time stamped so they could be correlated with the current and voltage measurements.

Two stainless steel plates 6.4 mm wide × 54 mm long lined the cathode flow channel and acted as the lands providing the electrical connection to the GDL. The anode lands consisted of six segments of stainless steel, 6.4 mm long and separated by 3.2 mm along the channel. The lead wires from each anode segment were connected individually to a 0.1 Ω sensing resistor to provide measurements of the local current density from the six positions along the flow channel. The six leads from the sensing resistors at the anode were connected together, and the common lead was connected through a 0–20 Ω, 10-turn potentiometer to the cathode, as diagramed in Figure 1 (a photo of the fuel cell and the experiment setup is available online at http://pemfc.princeton.edu/data.html). The sensing resistors were a total resistance of 0.016 Ω so that they contributed <3% to the total external impedance. We operated with a constant load resistance of 0.5 Ω.

The tubing from the gas flow channel outlets was bent down and bled into 10 mL graduated cylinders with a small hydrostatic head (~2–3 cm H_2O), so that the cell pressure was effectively 1 bar. Liquid in the cylinders kept air from back

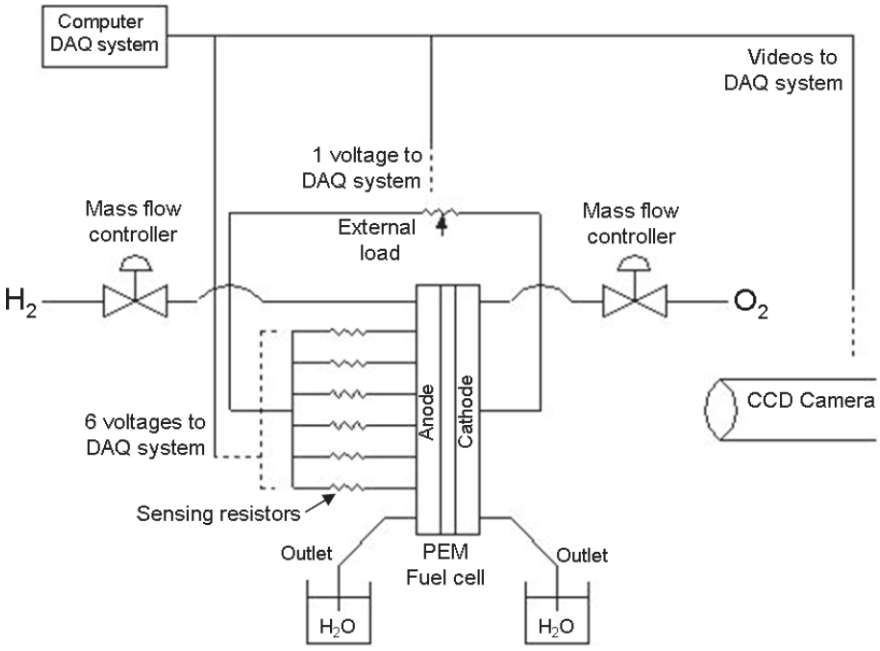

Fig. 1 Diagram of the SAPC Fuel Cell system showing the electrical circuit, DAQ connections, and peripherals.

diffusing into the flow channels. It also made it possible to see gas bubbles leaving the outlet tubes, which helped to identify the extent of reactant conversion in the fuel cell. The setup allowed for the flows at the anode and cathode to be either co-current or counter-current, with co-current flows chosen for all of the results presented here. We also chose to operate at room temperature at 20–25 °C. The vapour pressure of water was sufficiently low (~0.025 bar) so that convection of water vapour was negligible and almost all the water transport was by liquid flow.

The MEA was constructed in the lab from a Nafion 115 membrane, carbon cloth or carbon paper GDLs, and silicon gaskets. The GDLs were ELAT V2.1 obtained from E-TEK with the catalyst, 0.5 mg cm^{-2} of 20% Platinum on Vulcan XC-72, applied to one side. The dimensions of the electrodes were 5.72 cm long by 1.43 cm wide to give a total area of 8.17 cm^2. (Only 10%, 0.91 cm^2, of the MEA was exposed to the gas channel, the other 90% of the MEA was under the stainless steel electrodes). No microporous layer between the catalyst layer and GDL or at the flow channel-side of the GDL was used in these experiments.

2.2 Fuel Cell Orientation

A major advantage of the SAPC fuel cell design was the ability to operate the fuel cell in one of several possible orientations. With the choice of co-current flow, there were five different physical orientations (three horizontal and two vertical) which were defined by the effect that gravity had on liquid accumulation in the gas flow channel. The horizontal configurations were with the cathode facing downward and the anode facing upwards ('cathode down'), the cathode facing upwards and the anode downwards ('cathode up'), and the cathode and anode across from each other in the same horizontal plane ('horizontal'). In the 'cathode down' orientation, the force of gravity causes the droplets forming at the surface of the GDL to fall to the back of the flow channel. This occurs when they grow large enough such that the gravitational force overcomes the surface tension holding the drop to the water in the pore. The shear force from the gas flow must then push the droplets along the back of the flow channel to the outlets. The 90° bend at the outlet allows the drops to be easily removed, again with the help of gravity. The 'horizontal' orientation is similar in that the droplets grow until they detach and fall, but then they are pushed along the side of the flow channel and can partially block the flow of reactants into the GDL. Also, at the outlet, the 90° bend does not change the orientation with respect to gravity and the liquid water must continue to be pushed by the gas flow to be removed. The third horizontal orientation, 'cathode up', is opposite of 'cathode down' in that gravity holds the drops to the surface of the GDL. The force from the gas flows must overcome the surface tension holding the drop to the pore and must then push the water out of the outlet against gravity after the 90° bend.

The two vertical orientations were with the inlets at the top of the flow channel so that the gas flow was in the same direction as gravity ('inlets up') and with the inlets at the bottom of the flow channel so that gravity opposed the gas flow ('inlets down'). In the 'inlets up' orientation, gravity assists in both detaching the drops and moving the water to the outlets. The gas flow must then push the water out after the 90° for it to be completely removed. With the 'inlets down'orientation, the gas flow must also push the water after the bend at the outlet, but the water must first be pushed against gravity, the entire way up the flow channel to reach the outlet. Gravity helps to detach the drops but they fall down the flow channel towards the inlets where they can cause excessive flooding.

Figure 2 shows schematics of one of the horizontal orientations, (a) 'cathode down', and one of the vertical orientations, (b) 'inlets up'. The 90° bend at the outlets is shown clearly and water droplets are shown to demonstrate how they might grow as they move along the flow channel or detach and fall to the bottom.

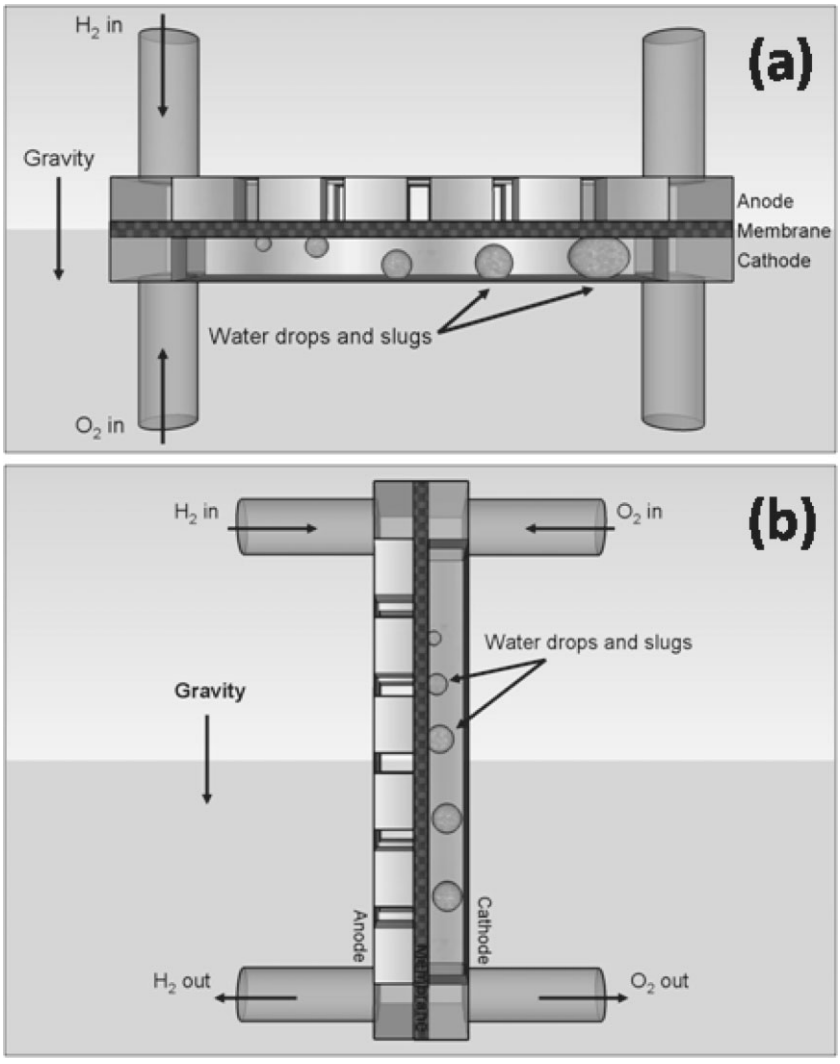

Fig. 2 Diagrams of two of the five possible orientations of the SAPC Fuel Cell. There are three horizontal orientations: the cathode facing up, the cathode facing down (shown in (a)), and the anode and cathode in the same horizontal plane. There are also two vertical orientations: the inlets at the top of the flow channel (shown in (b)) and the inlets at the bottom of the flow channel.

2.3 Fuel Cell Operation

Hydrogen and oxygen were never humidified and supplied directly from commercial cylinders through mass flow controllers at flow rates of 1–20 standard cubic centimeters per minute (sccm). There were also relative humidity sensors placed in the outlets from the gas flow channels to record any changes in the RH. In the experiments reported here, liquid water was always present in the flow channels and the RH in both the anode and cathode outlets was always 100% after a short start-up period.

The flow rates were chosen to understand the fuel cell operation under very high fuel conversion efficiency. This amplified the effects from gravitational forces and material properties relative to the effect of the shear force from gas flow. Furthermore, keeping the gas velocity in the flow channels low and the temperature low reduced the convective flow of water vapour. This permited water diffusion in the membrane and flow channel to humidify the membrane and allowed for operation with dry feeds. At steady state the water activity gradient is given as a balance of the convective flow of water in the gas flow channel with diffusion of water in the membrane and water diffusion in the gas flow channel as shown in equation 1 (the variable definitions and approximate values are given in Table 1).

$$\left(Q_{gas}^{A}+Q_{gas}^{C}\right)\frac{P_w^0}{RT}\frac{da_w}{dz}+\left(t_{mem}w_{ch}D_{w,mem}c_{w,mem}^{sat}+A_{ch}D_{w,gas}\frac{P_w^0}{RT}\right)\frac{d^2a_w}{dz^2}=\frac{j}{2F}\cdot w_{ch} \tag{1}$$

For a first approximation, we can neglect diffusion and consider only the balance between water production and convection. This allows for the calculation of the activity gradient along the flow channel, as given by equation 2,

$$\frac{da_w}{dz}=\frac{\frac{j}{2F}\cdot w_{ch}}{\left(Q_{gas}^{A}+Q_{gas}^{C}\right)\frac{P_w^0}{RT}} \tag{2}$$

The approximate values for the diffusivity of water in Nafion and the saturation water concentration in Nafion given in Table 1 were measured in our labs [15]. Including the diffusion terms makes the equation 1 much more complicated to solve than equation 2 due to how the properties of the membrane would change along the flow channel with changing water activity. Here we only consider equation 2, but accounting for diffusion would decrease the activity gradient as water would diffuse against the convective flow. Using values corresponding to the experimental fuel cell described earlier and typical flow rates for stoichiometries of 1-2, the water activity gradient is ~2.5 cm^{-1} at 25 °C, decreasing to ~0.46 cm^{-1} at 60 °C. The water activity decreases from outlet to the inlet; neglecting back diffusion the water activity in the SAPC fuel cell reaches 1, indicating saturated conditions, at 0.4 cm from the inlet at 25 °C and with dry feeds. At 60 °C, the length for saturation increases to ~2 cm, but the majority of the flow channel will still be exposed to saturated flow streams.

The maximum values the flow rates were fixed at were 12 sccm H_2 and 6 sccm O_2, corresponding to a stoichiometry of about 2 for the system described here. Through a series of

Table 1 Variable definitions and approximate values for symbols in equation 1

Variable	Definition	Approximate value
Q^A_{gas} / Q^C_{gas}	Flow rate of gas in the anode/ cathode flow channel	6/3 cm^3 min^{-1}
A_{ch}	Cross-sectional area of channel	0.05 cm^2
w_{ch}	Width of flow channel	0.1 cm
t_{mem}	Thickness of membrane	0.0127 cm
$D_{w,mem}$	Diffusion coefficient for water in the membrane	10^{-8} cm^2 s^{-1}
$D_{w,gas}$	Diffusion coefficient for water in the gas stream	0.2 cm^2 s^{-1}
P^0_w	Vapour pressure of water at the given temperature	0.032/0.20 bar @ 25/60 °C
$c^{sat}_{w,mem}\infty$	Saturation concentration of water in the membrane	15/30 mol cm^{-3} @ 25/ 60 °C
j	Current density	1 A cm^{-2}
F	Faraday's constant	96485 mol e$^-$ C^{-1}
R	Gas constant	83.145 cm^3 bar mol^{-1} K^{-1}
T	Fuel cell temperature	25/60 °C
a_w	Water activity	0–1 (calculated)
Z	Length dimension along the flow channel	0–5.7 cm

tests, we observed that with a load resistance of 0.5 Ω and flow rates of about 6/3 sccm H_2/O_2 (varying slightly with the MEA and state of the system), no gas bubbles were seen from the outlets of the anode and cathode, indicating complete conversion of the reactants. Figure 3 is a plot of the segmental currents and total fuel cell current and as a function of O_2 flow rate with the H_2/O_2 flow rate ratio kept constant at 2. The maximum total current from the SAPC fuel cell driving a 0.5 Ω load impedance at 25 °C and 1 bar total pressure was 0.88 A. For flow rates > 6/3 sccm H_2/O_2 the total current was almost independent of flow rate. Decreasing the flow rate to 6/3 sccm H_2/O_2 or lower resulted in a decrease in the total current delivered by the fuel cell, as evidenced by a change in slope of the current vs. flow rate curve. The net voltage changes at the same rate as the total current (with the constant load resistance of 0.5 Ω); however the absolute changes in the local currents indicate the local potential drops are not uniform along the electrodes.

We found variability in the internal resistance of about 10% from MEA to MEA, corresponding to variability in the total maximum current. The maximum flow rate where all the reactants were consumed by reaction is referred to as a stoichiometry (ξ) of 1, where ξ is the ratio of gas supplied through the feed to that consumed by the fuel cell with the given current. This point was easily identified by reducing the flow rates to the fuel cell and seeing when bubbles ceased to emerge from the fuel cell effluents. A reduction in the flow rate from $\xi = 1$ at the same load impedance reduces the total current; increasing the flow rates causes a negligible increase in the total current and results in gas bubbles emerging from the fuel cell. We will refer to the inlet flow rates giving complete consumption of the reactants as ξ_1, and 12/6 sccm H_2/O_2 as ξ_2. These are approximate stoichiometries of 1 and 2, respectively.

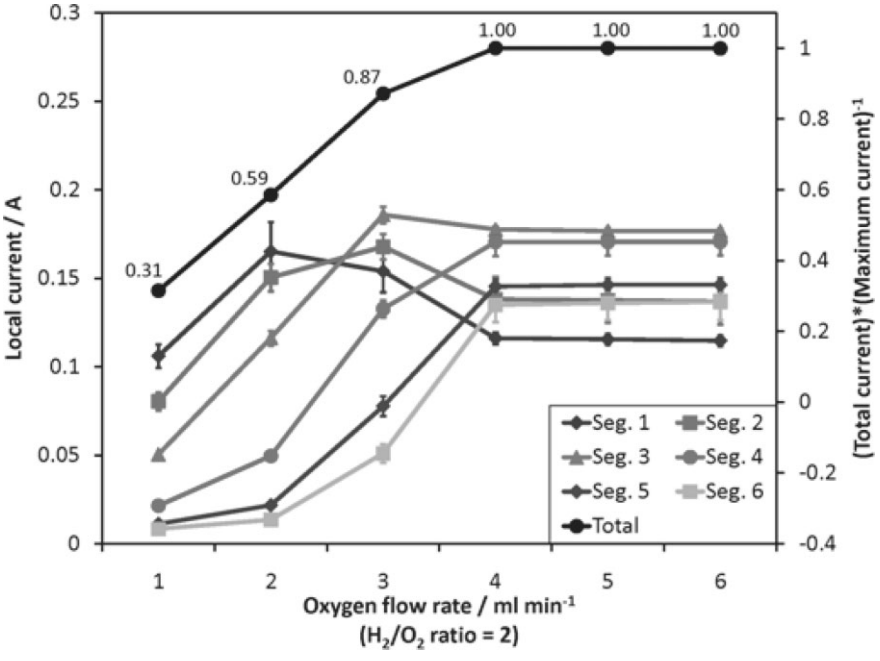

Fig. 3 Local and total currents (relative to the maximum total current) vs. O_2 flow rate (H_2/O_2 ratio constant at 2). Above 3 sccm O_2, the currents are independent of flow rate with a maximum total current of 0.88 A. At 3 sccm O_2 and below, the reactants are completely consumed. The fuel cell was in the vertical 'inlets up' orientation in order to minimise effects from liquid water accumulation. The data is the average from experiments with both increasing and decreasing the flow rates and starting from both dry and wet conditions.

2.4 Experimental Protocol

A typical experiment consisted of 3 stages, (1) startup with low reactant flow rates, (2) 'steady state' operation at excess stoichiometry and (3) 'steady state' operation at a stoichiometry of 1. The stages are indicated in Figure 4(a) by the change in flow rates (dashed lines) and are described in more detail below. The fuel cell was started for one hour with dry feeds of 6/3 sccm H_2/O_2; this was found to be sufficient to achieve a steady current in all the six anode segments. Referring to the water balance in equation 1, we see that using the low flow rate permits water diffusion to hydrate the membrane more effectively. After one hour the flows were increased to ξ_2 for two hours to allow the amount of water in the cell to equilibrate. At a current of 0.9 A, the time for liquid water to fill the cathode flow channel was 4000 s; one hour is thus a critical time constant for fuel cell operation and any characterisation of fuel cell operation should extend for several time constants.

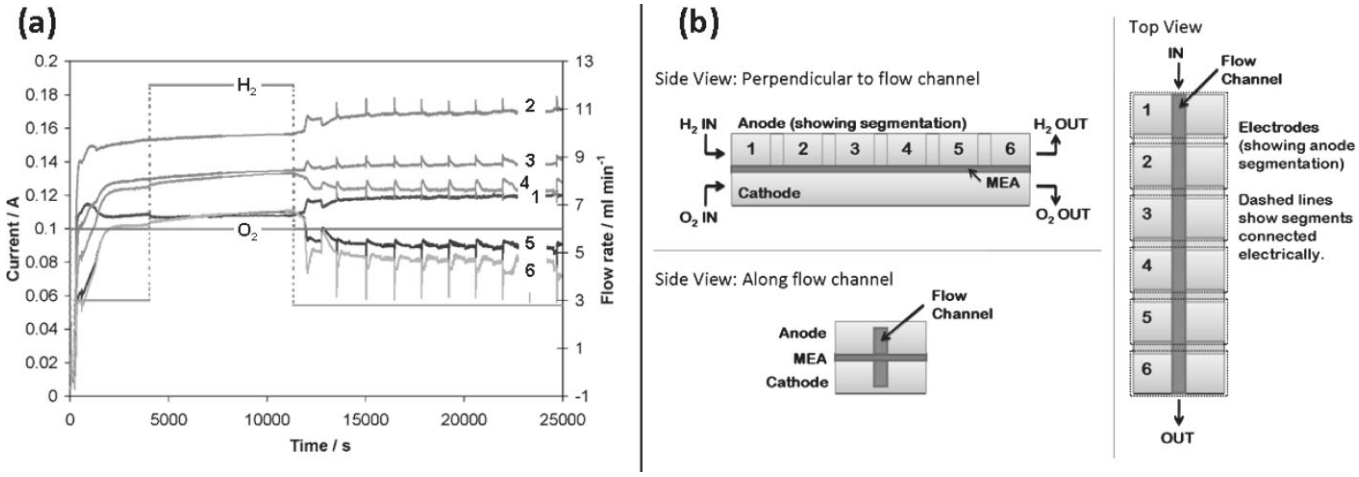

Fig. 4 (a) Raw spatio-temporal data from a typical experiment with the SAPC FC. The three stages are shown: start-up with low flow of 6 sccm H_2 and 3 sccm O_2, equilibration with 12 sccm H_2 and 6 sccm O_2, and starvation with complete consumption of reactants. Sharp fluctuations are observed when water slugs move through the flow channel. Parameters: cell temperature = 23 °C, load resistance = 0.5 Ω, orientation is horizontal 'cathode down' (see part (b)). (b) Schematic of the SAPC fuel cell in the 'cathode down' orientation (side views) showing the electrode segmentation. The flow channel is machined in the middle of the fuel cell such that the electrodes electrically connected across the channel.

Lastly, the flows were reduced to ξ_1 (~ 6/3 sccm H_2/O_2) for four hours. This highlighted the effects of liquid water accumulation and how the parameters of the system affected its removal, including the influence of gravity.

During the entire experiment, the reactant flow rates, voltage drop across the load resistor, and the current measurements from the six different anode segments were logged every second, as shown in Figure 4(a). 'Segment 1' was always defined as the anode segment closest to the feed inlets and 'segment 6' was always closest to the outlets, as shown in Figure 4(b). To mitigate the noise in the measurements, data samples were read from the data acquisition board at 16 Hz with the average over 16 samples saved to the data file at one point per second. With this, the fluctuations from noise in the data were kept acceptably low at no more than ±0.0001 A. (Typical current measurement for steady state operation was ~0.15 A per electrode segment, so the signal/noise ratio was >>100).

The data shown in Figure 4 was typical. After increasing the flows to ξ_2, the current measurements were stable, slowing increasing and finally leveling off. The current profile showed maximum current density at the centre of the flow channel (between position 2 and 3). The fall off in current at the flow inlet and outlet is the result of lateral currents through the MEA. When the flow rates were reduced to ξ_1, the currents showed some redistribution, with the currents near the inlet increasing modestly and the currents near the outlet decreasing. In most cases, the currents were stable between sharp periodic fluctuations caused by the movement of liquid water slugs (other cases showed continuously erratic fluctuations or sharp drop-offs in all of the currents).

2.5 Modified Gas Diffusion Layers

A single large pore was created in a carbon cloth GDL by poking a small pin all the way through the material. This created a pore with a diameter of about 400 µm, almost 3 times larger than the pores at the intersection of fiber bundle weave in carbon cloth that water would typically flow through [16]. The modified GDL was then used for the cathode side GDL in an MEA constructed as described in section 2.1. Figure 5 shows back-lit photos of GDLs with (a) the pore in a location that was under the channel and (b) the pore in a location that was under the land when the MEA was placed in the fuel cell. Overlays are given to show the relative location of the pores to the flow channel.

Figure 5(c) gives the diagram of the positions of the pore along the flow channel, relative to the segmentation of the anode (also refer to Figure 4(b)). The pore was created 19 mm from one end of the GDL. If that end was closer to the inlets, the pore was across the membrane from the space between segments 2 and 3 of the anode. If the pore was closer to the outlets, then it was across from the space between segments 4 and 5. The location of the pore proved to be very significant, as will be shown later.

3 Results

The work presented here focuses on how the structure of the GDL affects liquid water accumulation. We realise this is only one of the several factors; temperature and the properties of the flow channels are the subjects of continuing work in our group. Results will be presented in two ways. The first presentation is as line graphs of spatio-temporal data of the current measurements from the six different anode segments (such as that shown in Figure 4(a)). The flow rates of hydro-

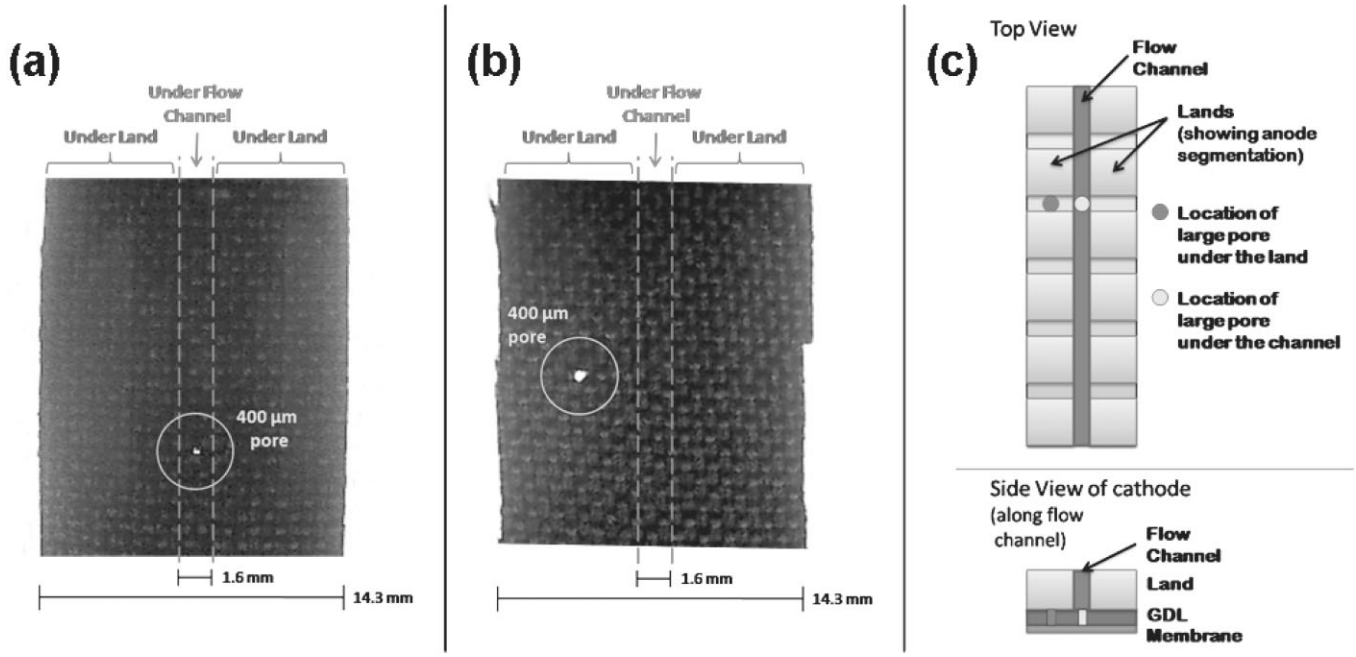

Fig. 5 Photos and schematic of modifications to the GDLs. The large pore is forced to be either under the channel or under the land, and closer to the inlets or closer to the outlets. (a) Backlit photo of a carbon cloth GDL with a large pore (circled in yellow) created to be under the channel. Overlay is given to show the areas that would be under the lands and channel in the fuel cell. (b) Backlit photo of a carbon cloth GDL with a large pore (circled in yellow) created to be under the land. Overlay is given to show the areas that would be under the lands and channel in the fuel cell. (c) Schematic showing the location of the large pores relative to the segmentation of the anode when the large pore is under the channel (yellow dot) and under the land (green dot).

gen to the anode and oxygen to the cathode are also given to associate changes in the local currents caused by changes in the flows. The second presentation is as 'current profiles', or the fraction of total current from each of the six segments along the flow channel. These are the steady-state currents taken over periods of ~100 s during which the local currents are 'stable'. In several configurations, the currents show sharp fluctuations, but we have used a snap-shot in time giving the steady values between fluctuations for the profiles. Further analysis of the fluctuations is given in the Discussion section.

3.1 Effects of Pore size

The most significant difference between carbon cloth and carbon paper GDLs is relevant to fuel cell operation as we have described it is the pore size distribution. The largest pores, the ones through which liquid water will flow, are about 140 µm in carbon cloth (these occur at the intersection of the weave of the fiber bundles). The largest pores through carbon paper are about 20 µm.[16] The adhesive energy between water in the pores and the water drops on the GDL surface scales with the cross-sectional area of the pore [14] so that the force to detach drops from the GDL pore is much greater for carbon cloth than the carbon paper. It is more likely that droplets emerging from the carbon cloth will span the flow channel, forming a slug prior to detachment, whereas smaller drops emerging from the carbon paper may be detached as individual drops. The shear force from the gas in the flow channel and the force from gravity both play a role in overcoming the surface energy to detach the droplets.

Figure 6 shows current profiles for two different fuel cell orientations, one horizontal: 'cathode down'(open symbols, dashed trendlines; shown in Figure 2(a)) and one vertical: 'inlets down'(filled symbols, solid trendlines; opposite vertical orientation from that shown in Figure 2(b)). Results are given at stoichiometries ξ_2 (part a) and ξ_1 (part b) and with MEAs made with both carbon cloth (diamonds) and carbon paper (circles). The data points give the averages over multiple experiments while the linear best-fit trendlines are given for clarity.

When the fuel cell was operated with excess gas flow, ξ_2, the orientation had only a small effect on the local current distribution. The current profiles, given in Figure 6(a), are relatively flat and the curves essentially lie on top of one another, indicating a uniform current distribution and minimal flooding. (There are some variations due to reproducibility of preparing MEAs and putting the fuel cell together). When the feed flow rates were reduced to ξ_1, the effects of gravity were amplified, as shown in Figure 6(b). With the horizontal 'cathode down' configuration, there is little change between Figures 6(a) and 6(b) and the dashed curves are relatively flat, indicating a uniform current distribution along the flow channel. Some starvation effects can be seen with the slight decrease in current at segments 5 and 6 (near the outlets), but

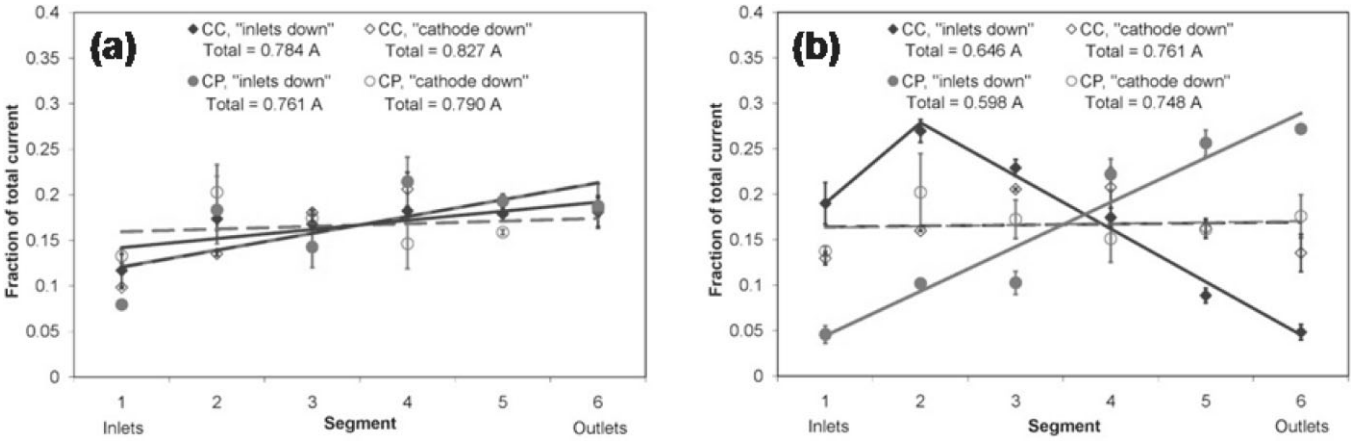

Fig. 6 Current profiles from experiments with both carbon cloth (diamonds) and carbon paper (circles) used in making the MEA and with the fuel cell in two different orientations, 'cathode down' (open symbols, dashed trendlines) and 'inlets down' (filled symbols, solid trendlines). The data points give the averages over multiple experiments while the linear best-fit trendlines are given for clarity. The error bars denote the standard error over multiple experiments. (a) Reactants supplied at ξ_2 (flows of 12/6 sccm of H_2/O_2) to give excess flows. (b) Reactants fully consumed with flows supplied at ξ_1 (~ 6/3 sccm H_2/O_2). Parameters for each experiment: cell temperature = 23 °C, load resistance = 0.5 **Ω**. Refer to Figure 2 for descriptions of the different orientations.

the surface of the GDL is left open for the oxygen to flow to the catalyst layer. It must be noted that there is a significant difference in the temporal dependence of the local currents between the high and low stoichiometries. As reported previously, the currents are temporally stable for ξ_2, but show large fluctuations at ξ_1. However, the steady values do not vary significantly. The reader is welcome to view the full spatio-temporal data sets online at http://pemfc.princeton.edu/SAPC/index.htm#meas.

In contrast, dramatic differences are seen in Figure 6(b) when gravity becomes more important and acts in the opposite direction of the gas flow; the current profiles for the carbon cloth are almost the inverse of that with the carbon paper. With the carbon cloth GDL, the currents are much higher towards the inlets with a peak at segment 2 and a sharp drop off towards the outlets. The profile results from slugs of water getting stuck at the top of the flow channel. The pores were large enough that the adhesion of the drops to water in the pore caused the droplets to span the flow channel and form a slug before detaching from the GDL. As the gas pressure increased behind the slugs, the oxygen was reacted to a greater extent upstream so that it was almost completely consumed near segments 5 and 6 and could no longer push the water slugs up against gravity. With the carbon paper GDL, we observed the opposite trend: low currents in the lower half of the channel and a sharp increase towards the upper segments. This resulted from water droplets detaching and falling to the bottom of the flow channel instead of forming slugs where the droplets emerged. The water collected at the bottom and blocked the flow of reactants to the segments closest to the inlets. The current redistributed towards the outlets as more oxygen was available to be consumed downstream.

3.2 Effects of GDL Modifications

A thorough understanding of how the properties of commercially available GDL materials affect water transport in the fuel cell suggested us to consider whether the pore sizes in the GDL could be exploited and actually control where and how the water emerges into the flow channels. To accomplish this, two carbon cloth GDLs were modified by creating a pore substantially larger than the intrinsic pores of the GDL, as described in section 2.5. Liquid water can move laterally between the GDL and catalyst layer seeking out the path of least resistance to flow, eventually leading to the largest pore. Water drops will emerge from the GDL at this large pore. In this paper we only report results for a carbon cloth GDL, where a single large pore at the intersection of the fiber weave was easily opened up from 140 to 400 μm (see Figure 5). When the large pore was under the channel, all of the liquid water emerged directly into the flow channel; interaction with the lands or channel walls occurred only after the emergent drop grew to span the channel. When the pore was under the land, the liquid water flowed through the GDL and entered the porous network between the GDL fiber weave and the flat stainless steel electrode. Liquid water moved along the interface between the GDL and land until it reached the flow channel, where it interacted with the surface of the stainless steel electrode making up one of the side walls of the channel. The stainless steel electrode was hydrophilic (contact angle ~ 15°) [17], in contrast to the hydrophobic carbon GDL (contact angle > 100°) [16] so that the water wicked onto the channel side walls and left the surface of the GDL clear.

Changing the liquid drop–surface interaction altered the importance of gravity, creating dramatic differences in the local current distribution between the different fuel cell con-

figurations. Figure 7 shows the results when gravity provided the most assistance in the removal of liquid water. The fuel cell was run in the 'inlets up' orientation (see Figure 2(b)), such that gravity assisted in removing the liquid water the entire length of the flow channel. Figure 7(a) gives the profiles of the current distribution with the flows at ξ_2. For each configuration of the MEA, the profiles are relatively flat and lie on top of one another. This indicates a uniform current distribution and minimal effects from liquid water accumulation. Figure 7(b) shows data from the same experiments shown in Figure 7(a), but after the flows were reduced to ξ_1 to give complete consumption of the reactants. Still, the profiles remain flat, with a small decrease in the currents towards the outlets due to reactant starvation. Again, as with the results given in Figure 6, significant differences were observed in the temporal data for the experiments shown in Figure 7. With excess flows, the currents were stable, but with the flows at stoichiometry ξ_1, sharp fluctuations occurred due to the movement of liquid water slugs in the flow channel. The 'steady'values (between the fluctuations) do not show significant differences, but the fluctuations themselves will be analysed later in the Discussion section. The full spatio-temporal data sets (showing the fluctuations) for all of the experiments presented in Figure 7 and the following Figure 8 can be viewed online at http://pemfc.princeton.edu/SAPC/index.htm#meas.

Rotating the fuel cell to the horizontal 'cathode up'orientation changed the influence of gravity so that it impeded liquid water removal, drastically changing the results. Figure 8 shows the steady-state current profiles for the fuel cell with the cathode facing up at stoichiometries ξ_2 and ξ_1 for different locations of the large pore. No steady state profile was obtained when the large pore was under the channel and near the inlet at ξ_1; this case will be reported separately. The cur-

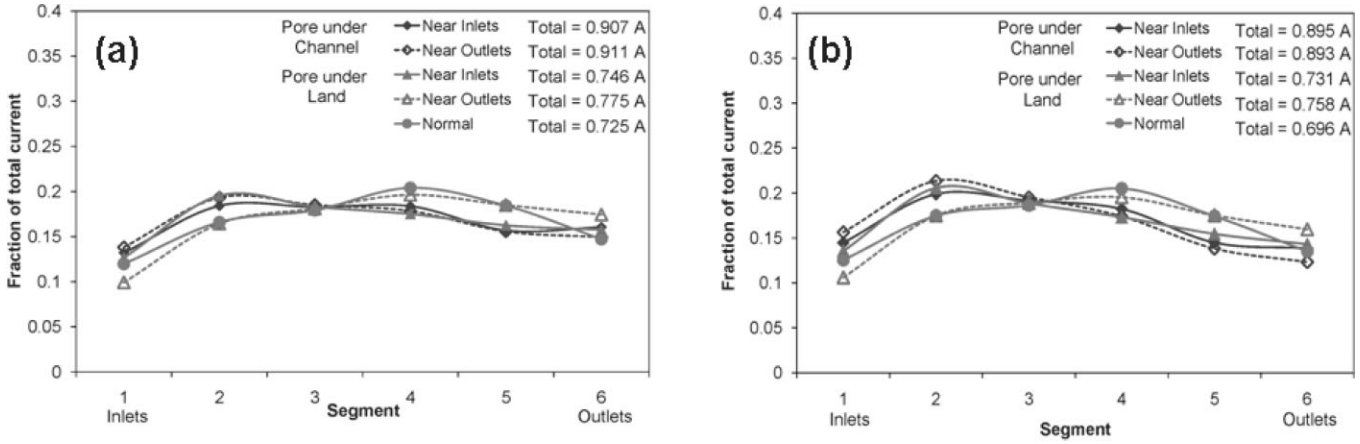

Fig. 7 Current profiles for the five different configurations of the MEA with carbon cloth GDLs (see Figure 5). The fuel cell was in the 'inlets up' orientation so that gravity assisted in removing the liquid water (see Figure 2(b)). The profiles are flat and lie on top of one another (a) with excess flows set at stoichiometry ξ_2 and (b) with complete utilisation of the reactants with the flows set at stoichiometry ξ_1. Parameters for all experiments: cell temperature = 23 °C, load resistance = 0.5 Ω.

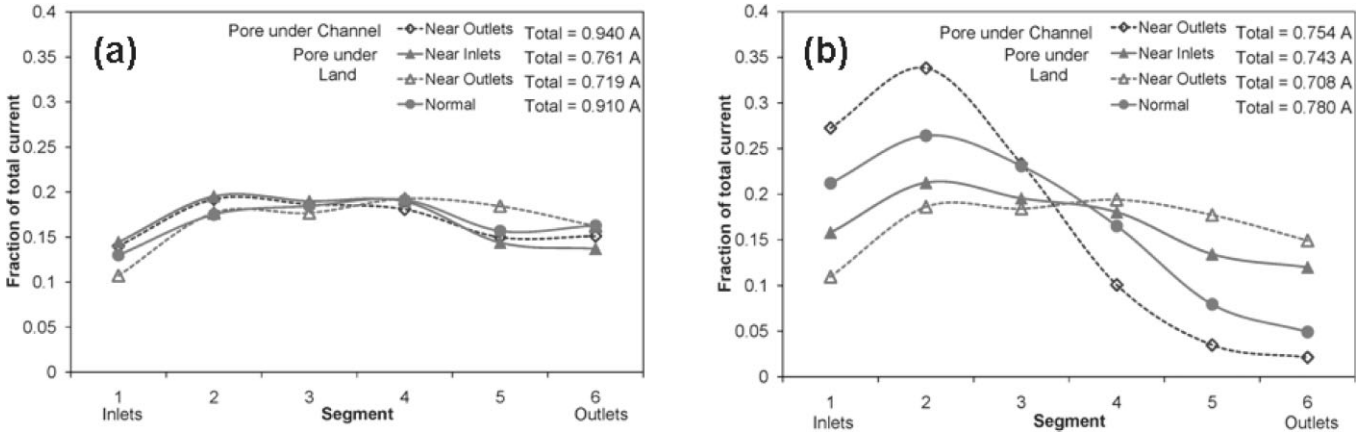

Fig. 8 Current profiles for four different configurations of the MEA with carbon cloth GDLs (results with the large pore under the channel and closer to the inlets not shown). The fuel cell is in the 'cathode up' orientation so that liquid water sits on the surface of the GDL as it is pushed along the flow channel and must be pushed against gravity to be removed through the outlets. (a) The profiles are flat and lie on top of one another with excess flows at ξ_2, but (b) dramatic differences are seen between the different configurations when the flows are reduced to ξ_1. Parameters for all the experiments: cell temperature = 23 °C, load resistance = 0.5 Ω.

rent profiles at the higher flow rates, ξ_2, shown in Figure 8(a) are very similar to Figure 7(a). The flow of the excess reactants diminished the effects of gravity in our small fuel cell so that the current profiles are flat and overlapping. Very different results are shown in Figure 8(b): when the flows were reduced to ξ_1 with the 'cathode up' orientation, the location of the large pore had a significant impact on the current profile. With the large pore placed under the land (triangles), either near the inlet or the outlet, the profiles are surprisingly flat. From visual observation, it appeared that as the water emerged between the GDL and land, it spread along the stainless steel and minimised the blockage of the pores at the surface of the GDL in the channel.

Placing the large pore under the flow channel and near the outlets caused the water to emerge and form drops in the flow channel. Without the aid of gravity to assist in detachment, the drops grew and spanned the gas flow channel. With all of the water flowing out of the single location, it covered the surface of the GDL near the pore, around segments 4, 5, and 6, creating a much higher resistance for the transport of oxygen into the GDL. The currents were much lower in that region and redistributed towards the inlets to give the sharp peak seen in Figure 8(b) (diamonds). The unmodified GDL (circles) had multiple locations where water broke through due to local pressure variations and many pores of similar sizes. Some water broke through under the land and some under the channel, indicated by how the profile curve lies right in between those for the two versions of modified GDLs.

The unusual results for the configuration with the horizontal 'cathode up'orientation (same orientation as for the data shown in Figure 8) and a large pore under the channel and near the inlets are shown in Figure 9. The fuel cell's performance progresses from start-up to a completely flooded state, indicated by a dramatic drop off in all of the local currents, with eventually only a partial recovery. The operation was with dry feeds (this is the case for all the data shown in this paper) and the flow rates were initially set low at 6/3 sccm H_2/O_2 so that the convective flow of water vapour was reduced enough to permit the dry membrane to hydrate. The currents ignited quickly as a result of the positive feedback between higher water production and increased membrane conductivity.[8] However, after approximately one hour, the currents in the fuel cell totally extinguished. The liquid water accumulated on the GDL surface, forming a slug and blocking the oxygen from getting into the GDL pores. The slug was pushed out of the flow channel but a film of liquid was left coating the walls, including the surface of the GDL. The oxygen flow to the cathode passed through the gas flow channel and never entered the GDL because of the liquid film. After one hour, the flows were increased to ξ_2, as done in all the other experiments. The fuel cell started to recover as the water film began to evaporate, but as more water was produced and pushed through the GDL, it added to the film at the surface and caused a secondary drop off in the currents, although not as severe as the initial failure. As the newly produced water emerged in flow channel at a much slower rate than in a non-flooded fuel cell and accumulated with an already present film, slugs did not form to cause fluctuations as in the typical experiment. Instead, we believe the thickness and coverage of the film changed until a balance was reached with the addition of product water into the film and the evaporation of water into the flow stream, as seen at about 7600 s in Figure 9. We also think, but do not have direct proof, that some liquid remained trapped between the GDL and the electrode (under the land) that reduced the diffusive oxygen transport laterally away from the flow channel, further contributing to the current production being unable to recover fully.

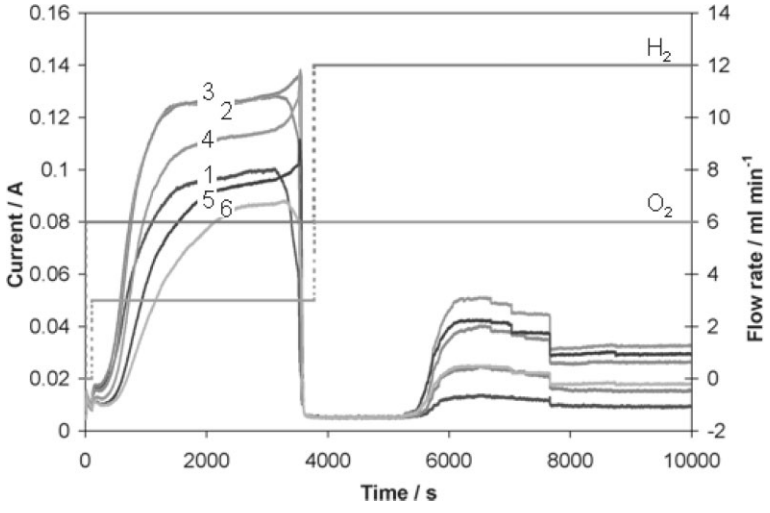

Fig. 9 Spatio-temporal data of the current measurements from the six different anode segments with the fuel cell in the 'cathode up' orientation and a large pore under the channel and closer to the inlets.

4 Discussion

Several factors affect the movement of liquid water in the flow channels; temperature, gas flow rate, hydrophobicity of the pores, surface tension between the water and the channel walls, flow channel design, and flow channel orientation. A number of recent investigations have looked at where water is formed and how it moves in PEM fuel cells. The results we present here begin to make connections between where liquid water accumulates and the local current density in PEM fuel cells. Our results also show that the structure of the GDL can be modified to control water movement on a macroscopic scale to benefit fuel cell operation. The directing of water motion through the GDL into specific areas of the gas flow channel may be exploited to improve the efficiency of PEM fuel cells. Although, the SAPC fuel cell is not a standard fuel cell design and has not been optimised for effi-

ciency, it provides detailed information about the physics and chemistry of the fuel cell and its components that can be employed to design efficient fuel cell systems.

The observations of liquid drops and slugs in PEM fuel cell flow channels by direct visualisation, MRI, and other methods has prompted several groups to study the behaviour of liquid water and flooding in PEM fuel cells with various numerical methods. Some of the work has focused on the flow channels, including studies on the dynamics of water droplet deformation and detachment [18–20], the effects of the hydrophilicity/hydrophobicity of the channel walls [21], and the geometry of the flow field [22, 23]. Others have looked at the gas diffusion layer with goals of understanding the differences between carbon cloth and carbon paper [24] and the mechanism for water transport into and through the GDL [25–28]. However, we are unaware of any studies that have considered the role of where liquid emerges from the GDL on the local current density in the PEM fuel cell. There has also been limited effort to examine the role of gravity and fuel cell orientation on performance. The work in our group has continued to show the importance of these factors.

Because of the limited understanding of liquid water accumulation and motion, the designs for fuel cells have been limited to heuristics. A few groups have developed novel strategies for managing the liquid water after it has been transported into the flow channels. Passive techniques using material properties are the most desirable to minimise parasitic power loss and keep the system cost and size down. Honda has simply used parallel straight channels in a vertical orientation with the feeds at the top so that the liquid water is removed by gravity [29], similar to how we most easily obtain stable operation with our SAPC design and low flow rates. Hogarth and Benziger introduced the concept of gravity assisted draining with a channel-less flow design to achieve improved PEM performance with dry feeds at elevated temperatures [13]. Woo and Benziger demonstrated that gravity draining could be employed to change the active area of a PEM fuel cell for load following control [30]. Investigations of several other novel flow field designs, including interdigitated and tapered flow fields, have shown improvements in performance, usually due to increased convection along the flow channel and through the GDL [31–36].

Several companies and patents have introduced active approaches to control water motion. One has been to use porous materials for the bipolar plates in a stack, such that liquid water is pulled from the flow channels into the coolant channels through a pressure differential [37]. Another has been to use hydrophilic porous flow field plates to wick water away from the GDL, with the excess water removed through an external electro-osmotic pump [38]. Each of these has clear advantages, but also the disadvantage of increased power demands and equipment in the system. The lack of details about the local current density and the dynamics of the water motion limit the opportunity to optimise these designs. A thorough understanding of how to control the location of water accumulation affects the fuel cell performance, especially through spatio-temporal data, and provides new insight for improved fuel cell design.

The key results obtained from the results with the different MEAs, fuel cell orientations and flow rates are summarised below:

1. Liquid water moves from the catalyst/membrane interface to the flow channel/land through the largest pore in the GDL. When the largest pore is under the flow channel, liquid drops appear in the flow channel and grow until they are detached from the combined forces of gravity and shearing from the gas flow. When the largest pore is under the land, the liquid water emerges into the flow channel at the corner between the GDL and the flow channel and land and can be transported along the channel side walls.
2. Flooding occurs when liquid water in the cathode flow channel spans the flow channel or covers the surface of the GDL, hindering oxygen from entering the GDL. Flooding is a local phenomenon that is spatio-temporal dependent; the location of flooding changes as liquid slugs move in the flow channel.
3. Gravity plays a key role in flooding. When liquid flow is assisted by both gravity and gas flow, the fuel cell runs stably and flooding is only observed at very low gas flow rates – near the outlets of the flow channels under starved conditions. When gravity acting on liquid drops and slugs is opposed to the gas flow, liquid accumulates, building up large slugs that shut down the local current in the fuel cell.
4. Drops emerging in the flow channel are held in place by the adhesion force to the liquid in the GDL pore. Drops emerging from small pores (< 25 μm), such as those found in carbon paper, form small drops that can be detached by the gas flow shear. Drops emerging from large pores (> 100 μm) grow to mm size and appear to span the gas flow channel before they are detached by inertial forces of the gas flow applied to liquid slugs.

Liquid water accumulation results in local current density variations. In addition to spatial current distributions, water motion causes temporal fluctuations of the current. These fluctuations have implications for power conditioning as the controller must be able to compensate for any sudden sharp changes without a significant interruption in the power being delivered. The effects of local starvation are evident in the redistribution of the currents during the fluctuations; as a slug causes the local currents to drop towards the outlets, those close to the inlets increase (see Figure 4). Degradation of the MEA may also be exacerbated as lateral voltage differences are induced that drive corrosive reactions. Looking more closely at the fluctuations in the local currents provides additional information about the mechanisms of liquid slug motion and why one fuel cell design might be better than another.

4.1 Frequency of Current Fluctuations

Both the magnitude and frequency of the fluctuations can be compared for the different configurations of the SAPC fuel cell. Figure 10 compares the frequency of current fluctuations for three different orientations and the six configurations of the MEA discussed earlier (including a carbon paper GDL). The three orientations have varying degrees of influence from gravity: horizontal 'cathode up', such that water sits on top of the GDL and must be removed against gravity at the outlets (black); horizontal 'cathode down', such that gravity assists as the water droplets detach from the GDL and fall to the back of the flow channel but then must be pushed out by the gas flow (white); and vertical 'inlets up', such that gravity assists in liquid water removal along the entire flow channel (grey). The boxes indicate the average frequency of fluctuations over at least 5 fluctuations, while the error bars indicate the maximum and minimum frequency between two fluctuations.

With most of the configurations, as the assistance from gravity in removing water increases, so does the frequency of fluctuations. The vertical 'inlets up' orientation, which has gravity acting in concert with the gas flow, has the highest frequencies. The horizontal 'cathode down' has the next highest frequencies, where gravity assists in the removal of liquid from the surface of the GDL. The lowest frequencies were observed for the horizontal "cathode up" orientation. In the horizontal 'cathode up' orientation, the outlet has a 90° angle from horizontal to vertical where water collects and causes a back-up in the gas flow before being removed from the fuel cell.

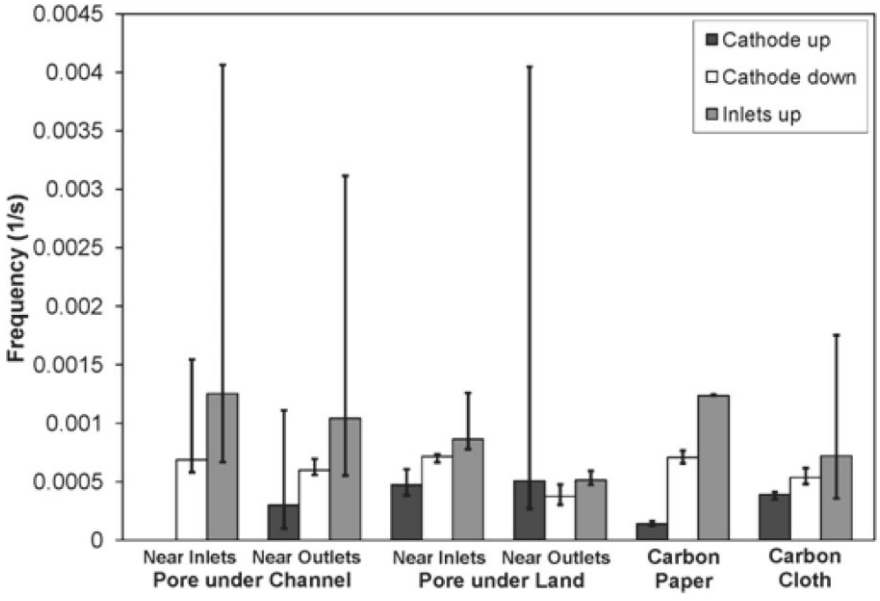

Fig. 10 Comparison of the frequency of fluctuations with the fuel cell in three different orientations and with six different configurations of the MEA (including a carbon paper GDL). The average over several fluctuations is given with the error bars indicating the maximum and minimum frequency between two fluctuations.

The large error bars with some of the configurations indicate more erratic fluctuations and inconsistent slug movement. With the 'inlets up'orientation, gravity and the shear force from the gas flow acted in the same direction to deform the water droplets as they grew, changing how frequently they spanned the channel to form slugs. This effect was the most significant for the configurations with the large pore under the channel as the droplets were relatively large and formed directly in the channel. The deformation of the droplets could act to both help slugs form or elongate the droplets down the channel, causing the varied times between the fluctuations. Another factor was drop coalescence. Droplets forming higher in the channel, on the surface of the GDL or from condensation on the channel walls, were pushed down the channel by both gravity and shear forces and could coalesce with other droplets to irregularly increase the frequency of the fluctuations. With the carbon paper and the smaller droplets that formed at the surface, the converse was true; the smaller droplets were detached from the GDL much easier and were less affected by coalescing with other droplets, thus the variance bars are much smaller.

The other configuration with a large error bar is with the large pore under the land, closer to the outlets, and in the 'cathode up' orientation. In that case, the water that emerged into the flow channel from under the land could accumulate with residual water not removed by previous slug movement. This could then form a slug in a shorter amount of time, causing fluctuations at higher frequencies. This effect was probably not observed when the large pore was under the land but near the inlets as the water emerged earlier in the channel and spread out along the channel walls instead of forming a slug.

The frequency of the fluctuations is controlled by the time for water accumulation to form a slug; this was determined largely by the current, but was also affected by how much accumulated water was pushed out with each slug. The frequency of the fluctuations was ~10^{-3} Hz, approximately the time to fill a substantial fraction of the flow channel with liquid water. The fraction of the flow channel that was filled with liquid varied for the different configurations. Residual water after slugs were pushed out of the flow channel reduced the time necessary to form a new slug. Slugs would break up as they went around corners or through fittings, allowing the gas to flow by while pushing out only part of the water. In fuel cells with different flow field designs, this would be expected to happen around corners or at junctions where the geometry or diameter might change. Also, corners and junctions can

change the orientation of the flow channel with respect to gravity, disrupting the flow of liquid water or creating areas where water can collect more easily, thus increasing the frequency of fluctuations.

4.2 Magnitude of Current Fluctuations

The magnitude of the fluctuations was defined as the integrated deviation in the total current, averaged over several fluctuations. Figure 11 gives the magnitudes for the same orientations and configurations as shown in Figure 10. The magnitude generally varied inversely to the frequency – the product of frequency and magnitude was approximately constant to within a factor of 2.

Large variations in the magnitude of the fluctuations are seen between the different configurations and were larger for carbon cloth than carbon paper (noting the log scale on the vertical axis). The largest fluctuations were observed for the large pore under the flow channel with the cathode facing up; this corresponds to the situation where gravity was an impediment to slug removal. The most extreme case was the horizontal 'cathode up'orientation with the pore under the channel near the inlet; this situation resulted in the shutdown of the current when a liquid film was left behind, covering the GDL, that only eventually partially recovered (see Figure 9). When the large pore was situated under the land, the effects of orientation and location were minimised; the magnitudes are relatively constant across the different orientations. The channel walls were more hydrophilic than the surface of the GDL, so the water wicked onto the walls as it seeped out under the land and reached the channel. It could then flow along the walls in larger, spread out drops or as a film and not hinder gas flow into the GDL, regardless of the orientation of the flow channels.

4.3 Considerations for Design

The trends in the frequency and magnitude between the different orientations have only been described semi-quantitatively. Neither the steady-state operation nor the fluctuations are deterministic. The spatio-temporal current patterns show variations from the way in which water drops accumulate to form slugs and how the slugs move and break apart. Still, the results that have been discussed have implications for application-specific designs for PEM fuel cells, an issue not widely discussed in the literature. With some applications, such as portable power, the orientation of the fuel cell system might change suddenly (it could be dropped, kicked over, or the person wearing a fuel cell pack might fall over). An MEA configuration which is less sensitive to orientation would be very beneficial. Often, and most notably with the carbon paper, the magnitude of the fluctuations are very small in one orientation, but much larger in another. This could be very problematic when designing a controller for the fuel cell system if the configuration was chosen that minimised the fluctuations. If the system is only capable of compensating for very small changes but then the orientation becomes one where large fluctuations occur, the entire system could fail. Other applications, automotive for example, will be much more stable with respect to the orientation so that the system could be optimised with only minimum fluctuations expected.

The fluctuations and slug movement may also be further controlled by tailoring the pore size distribution with the

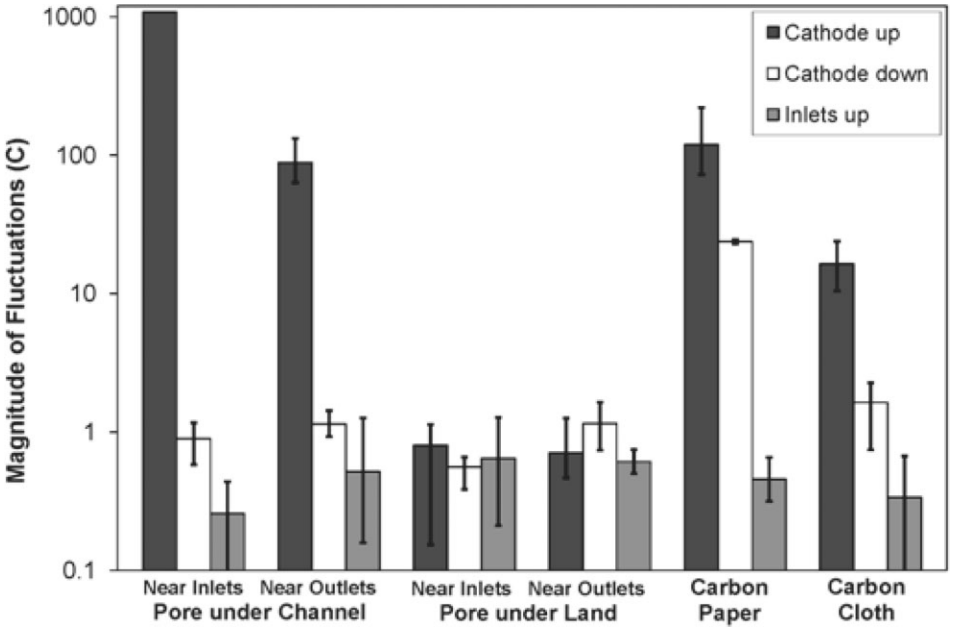

Fig. 11 Comparison of the magnitude of the fluctuations with the fuel cell in three different orientations and with six different configurations of the MEA (including a carbon paper GDL). The average over several fluctuations is given with the error bars indicating the maximum and minimum magnitude.

application and fuel cell orientation in mind, allowing for slugs to form more or less frequently. For example, the data for the 'inlets down' orientation in Figure 6(b) alludes to possible benefits of a 'hybrid'GDL with larger pores in the lower half of the GDL, closer to the inlets, and smaller pores in the upper half, closer to the outlets. In that case, slugs should form at the bottom of the flow channel and clear liquid water as they are pushed up and out of the flow channel in a predictable way.

As a final consideration, we have observed that defects in the flow channels caused water to build-up in a certain location. This causes larger slugs to form and the force needed to push the water past the defect is greater than that needed to push the water along a smooth channel. When the slug is finally removed, the resulting fluctuation may be much larger than expected. Another group has also reported results on water collecting at defects seen with MRI, but did not discuss the effects on the fuel cell performance [39]. Defects and other properties of the flow channels, such as the hydrophilicity or roughness of the channel walls, significantly influence the fuel cell performance and are the subjects of continuing work in our group.

4.4 Force Balance for Droplet Detachment

As mentioned previously, droplets are detached from the surface of the GDL by overcoming the surface tension between the water in the droplet and the water in the pore. Both the shear force from the gas flow and gravity contribute to detachment, but only act in the same direction with one of the orientations, vertical 'inlets up'. For the horizontal orientation 'cathode down', gravity assists in removing the drops from the GDL surface but the gas flow must push the liquid out of the flow channel. In the horizontal orientation 'cathode up', gravity acts to hold the drops on top of the surface of the GDL while the shear force acts to detach the drops and push them along the flow channel. Finally, in the vertical orientation 'inlets down', gravity and shear forces oppose each other with the flows going upwards and gravity pulling the droplets back towards the inlets. With these orientational dependences in mind, we can write the simple force balance for water drop detachment from the GDL (equation 2).

$$\text{water surface tension} = \text{force from gravity} \pm \text{shear force}() \tag{3}$$

$$2\pi r_{pore}\gamma_{water} = \frac{4}{3}\pi r_{drop}^3 \rho_{water} g \pm \left(\frac{4\mu_{gas}Q_{gas}}{\pi r_{channel}^3}\right)\left(\pi r_{drop}^2\right)$$

where r is the radius, γ is surface tension, μ is viscosity, Q is volumetric flow rate, ρ is density and g is the acceleration due to gravity. To fully capture the orientational effects, equation 2 should be written separately for each orientation as a three-dimensional vector equation, but here we have simply used the ± symbol to denote the different ways the two forces can act relative to each other.

When choosing a GDL material and designing flow channels, one wants to know if the water drops will span the flow channel and form slugs or remain as drops. Based on GDL pore diameters of 20 μm for carbon paper and 140 μm for carbon cloth, the predicted size for drop detachment due to gravity is 0.6 mm for carbon paper and 1.2 mm for carbon cloth. With the parameters of the SAPC FC ($Q_{gas} \sim 10^{-7}$ m^3 s^{-1}, $r_{channel} \sim 1$ mm), droplets will be detached before spanning the flow channel for both the carbon cloth and carbon paper in the vertical 'inlets up' orientation, where the gas flow is assisted by gravity. When the flow channel orientation is horizontal 'cathode down', gravity again will assist the detachment of the drops from the GDL. However, because gravity does not assist in pushing the drops along the flow channel, at low stoichiometry the drops will aggregate as they move along the flow channel and form slugs near the outlet. In the horizontal 'cathode up' orientation, the shear forces are insufficient to detach drops emerging from the carbon cloth GDL, resulting in slug formation at the location of the largest pores that blocks the gas flow. With a carbon paper GDL used in the horizontal 'cathode up' orientation, the drops emerging from the GDL can be detached by the gas flow before spanning the channel, but they will aggregate with other drops as they move down the channel and form slugs near the outlet. The significance of this analysis is that without the force from gravity or constraints of the channel walls, the droplets would grow to a radius exceeding the dimensions of the flow channel before the shear force would overcome the surface tension.

The force balance in equation 2 assumed spherical droplets. As the droplets are deformed by the forces or come into contact with the sides of the flow channel, this assumption is no longer valid. Furthermore, as the droplets grow and block a significant fraction of the channel cross-sectional area, the velocity of the gas will increase as it flows through the smaller space and cause a greater deformation by shear force than what equation 2 predicts. These factors will change the calculation of when slugs are formed and have the added complexity of the possibility for water film formation, but is beyond the scope of the analysis presented here.

5 Conclusions

The pore structure of the GDL directs the positions where water emerges into the gas flow channels. We have demonstrated for the first time that the pore structure of the GDL can be modified to force water to emerge at specific locations. The location of the emergent water with respect to the location in the channel or under the land, the local gas flow velocity, the orientation of the fuel cell with respect to gravity, and the surface properties of the gas flow channel determine how large drops or slugs form, whether drops span the flow channel, and what the local current density is in the fuel cell. We have shown that proper location of the water flow pores in the GDL can minimise the local current fluctuations in the fuel cell.

The differences between carbon cloth and carbon paper are significant and largely due to the differences in the sizes of the water droplets that emerge at the surface. With much larger pores, the droplets that form with the carbon cloth span the channel more easily to form slugs that are then pushed along by the gas flow. With carbon paper, the droplets are smaller and more likely to detach from the GDL before spanning the flow channel. This can be exploited using straight flow channels oriented down where gravity assists the drainage; such designs have been adopted by Honda. The Honda design is not good for operation with dry feeds. When operating with dry feeds, where it is desirable to reduce the flow rate and have liquid in the cell mix with the reactants, carbon cloth will be better for operation.

Beyond examining how liquid water is transported through the GDL and into the cathode flow channel, we showed that the GDL can be modified to direct the location of where liquid water will emerge from the GDL. When water was directed to emerge into the flow channel, water slugs formed that spanned the channel and caused large fluctuations in the local current density. The magnitude of the fluctuations was reduced by locating the pores for liquid transport under the land. It is now possible to consider coupling the design of both the GDL and flow fields for specific applications.

Acknowledgements

We thank the National Science Foundation (CTS -0754715) for supporting this work. E. Kimball also thanks the Princeton University Program in Plasma Science and Technology for partial support under U.S. Department of Energy Contract No. DE-AC02-76-CHO- 3073.

References

[1] C. Yang, S. Srinivasan, A. B. Bocarsly, S. Tulyani, J. B. Benziger, *J. Membr. Sci.* **2004**, *237*, 145.
[2] J. P. Owejan, T. A. Trabold, D. L. Jacobson, D. R. Baker, D. S. Hussey, M. Arif, *Int. J. Heat Mass Transfer* **2006**, *49*, 4721.
[3] K. Tuber, D. Pocza, C. Hebling, *J. Power Sources* **2003**, *124*, 403.
[4] A. Turhan, K. Heller, J. S. Brenizer, M. M. Mench, *J. Power Sources* **2006**, *160*, 1195.
[5] M. A. Hickner, N. P. Siegel, K. S. Chen, D. S. Hussey, D. L. Jacobson, M. Arif, *J. Electrochem. Soc.* **2008**, *155*, B294.
[6] J. Stumper, C. Stone, *J. Power Sources* **2008**, *176*, 468.
[7] X. Z. Yuan, J. C. Sun, M. Blanco, H. J. Wang, J. J. Zhang, D. P. Wilkinson, *J. Power Sources* **2006**, *161*, 920.
[8] J. B. Benziger, E. S. Chia, Y. De Decker, I. G. Kevrekidis, *J. Phys. Chem. C* **2007**, *111*, 2330.
[9] F. Y. Zhang, X. G. Yang, C. Y. Wang, *J. Electrochem. Soc.* **2006**, *153*, A225.
[10] Z. Dunbar, R. I. Masel, *J. Power Sources* **2007**, *171*, 678.
[11] S. Litster, D. Sinton, N. Djilali, *J. Power Sources* **2006**, *154*, 95.
[12] D. Gerteisen, T. Heilmann, C. Ziegler, *J. Power Sources* **2008**, *177*, 348.
[13] W. H. J. Hogarth, J. B. Benziger, *J. Power Sources* **2006**, *159*, 968.
[14] E. Kimball, T. Whitaker, Y. G. Kevrekidis, J. B. Benziger, *AIChE J.* **2008**, *54*, 1313.
[15] P. W. Majsztrik, M. B. Satterfield, A. B. Bocarsly, J. B. Benziger, *J. Membr. Sci.* **2007**, *301*, 93.
[16] J. Benziger, J. Nehlsen, D. Blackwell, T. Brennan, J. Itescu, *J. Membr. Sci.* **2005**, *261*, 98.
[17] J. T. Givens, in *Chemical Engineering*, Vol. B. S. E., Princeton University, Princeton **1999**, 64.
[18] X. Zhu, P. C. Sui, N. Djilali, *Microfluid. Nanofluid.* **2008**, *4*, 543.
[19] A. Golpaygan, N. Ashgriz, *Int. J. Comput. Fluid Dyn.* **2008**, *22*, 85.
[20] A. Theodorakakos, T. Ous, A. Gavaises, J. M. Nouri, N. Nikolopoulos, H. Yanagihara, *J. Colloid Interface Sci.* **2006**, *300*, 673.
[21] Y. H. Cai, J. Hu, H. P. Ma, B. L. Yi, H. M. Zhang, *J. Power Sources* **2006**, *161*, 843.
[22] A. Kumar, R. G. Reddy, *J. Power Sources* **2003**, *113*, 11.
[23] C. Xu, T. S. Zhao, *Electrochem. Commun.* **2007**, *9*, 497.
[24] Y. Wang, C. Y. Wang, K. S. Chen, *Electrochim. Acta* **2007**, *52*, 3965.
[25] P. K. Sinha, C. Y. Wang, *Electrochim. Acta* **2007**, *52*, 7936.
[26] G. L. He, P. W. Ming, Z. C. Zhao, A. Abudula, Y. Xiao, *J. Power Sources* **2007**, *163*, 864.
[27] Z. X. Liu, Z. Q. Mao, C. Wang, *J. Power Sources* **2006**, *158*, 1229.
[28] H. Meng, C. Y. Wang, *J. Electrochem. Soc.* **2005**, *152*, A1733.
[29] T. Komura, T. Moriya, S. Isobe, T. Ushiro, *United States Patent 6, 242, 119*, **2001**.
[30] C. H. Woo, J. B. Benziger, *Chem. Eng. Sci.* **2007**, *62*, 957.
[31] A. Turhan, K. Heller, J. S. Brenizer, M. M. Mench, *J. Power Sources* **2008**, *180*, 773.
[32] X. D. Wang, Y. Y. Duan, W. M. Yan, X. F. Peng, *Electrochim. Acta* **2008**, *53*, 5334.
[33] H. C. Liu, W. M. Yan, C. Y. Soong, F. Chen, H. S. Chu, *J. Power Sources* **2006**, *158*, 78.
[34] A. Kumar, R. G. Reddy, *J. Power Sources* **2004**, *129*, 62.
[35] W. M. Yan, C. Y. Soong, F. L. Chen, H. S. Chu, *J. Power Sources* **2004**, *125*, 27.
[36] T. V. Nguyen, *J. Electrochem. Soc.* **1996**, *143*, L103.
[37] J. S. Yi, J. D. L. Yang, C. King, *AIChE J.* **2004**, *50*, 2594.
[38] S. Litster, C. R. Buie, T. Fabian, J. K. Eaton, J. G. Santiago, *J. Electrochem. Soc.* **2007**, *154*, B1049.
[39] Z. W. Dunbar, R. I. Masel, *J. Power Sources* **2008**, *182*, 76.

